Journal of Industrial and Engineering Chemistry 110 (2022) 414–423

Contents lists available at ScienceDirect

Journal of Industrial and Engineering Chemistry

journal homepage: www.elsevier.com/locate/jiec

Enhanced mechanical properties of epoxy composites embedded with MF/TiO_2 hybrid shell microcapsules containing n-octadecane

Guangjian Peng [a,b], Yahao Hu [a], Guijing Dou [a], Yiheng Sun [a], Yong Huan [c,d], Sung Hoon Kang [b,*], Zhongyu Piao [a,*]

[a] College of Mechanical Engineering, Zhejiang University of Technology, Hangzhou 310023, China
[b] Department of Mechanical Engineering and Hopkins Extreme Materials Institute, Johns Hopkins University, Baltimore, MD 21218, USA
[c] State Key Laboratory of Nonlinear Mechanics (LNM), Institute of Mechanics, Chinese Academy of Sciences, Beijing 100190, China
[d] School of Engineering Science, University of Chinese Academy of Sciences, Beijing 100049, China

ARTICLE INFO

Article history:
Received 23 January 2022
Revised 7 March 2022
Accepted 14 March 2022
Available online 19 March 2022

Keywords:
In situ polymerization
Hybrid shell microcapsules
Microcapsule/epoxy composites
Interface strengthening

ABSTRACT

Microencapsulated phase change materials (MPCMs) are often mixed with matrix materials to form phase change composites for energy storage. Typically, MPCMs are easily debonded from the matrix or ruptured, thereby weakening the mechanical properties of composites. This paper aims to simultaneously improve the rupture strength of microcapsules and the bonding strength between microcapsules and matrix to enhance the mechanical properties of composites. The titanium dioxide (TiO_2) nanoparticles modified by a silane coupling agent (KH560) were doped into the melamine formaldehyde (MF) shell, forming n-octadecane@MF/TiO_2 hybrid shell MPCMs (HS-MPCMs). The doping of modified TiO_2 nanoparticles reduced supercooling and improved the thermal stability of microcapsules. Compared with MF microcapsules, the rupture strength of HS-MPCMs was increased by an average of 30.4%. The modified TiO_2 nanoparticles also built covalent bonds between microcapsule shell and matrix, which led to better microcapsule/epoxy interface bonding. Thus, the HS-MPCMs/epoxy composites performed higher tensile strength than the unmodified composites. Specifically, the tensile strength of composites was improved by an average of 17.2% at the microcapsule content of 10 wt.% with the aid of the MF/TiO_2 hybrid shell. The reinforced MPCMs/epoxy composites are expected to be used as anti-icing coatings in the aerospace field.

Introduction

Materials that can autonomously store and release thermal energy provide great opportunities for efficient and compact thermal energy management. As carriers of latent thermal energy, phase change materials (PCMs) implement storage and release of thermal energy through phase transition [1,2]. PCMs can greatly improve energy efficiency compared with sensible heat storage and have attracted widespread attention in the energy field. Microencapsulated phase change materials (MPCMs) utilize a film-forming material to coat PCMs for forming microspheres with core–shell structure to prevent the leakage of melting PCMs and increase the heat transfer area [3–5]. MPCMs have broad application prospects in the fields of construction [6–8], aerospace coatings [9–11], and textiles [12,13]. MPCMs are mixed with matrix materials such as epoxy, gypsum, and foam to form the phase change composites for energy storage and intelligent temperature regulation [14,15]. In practical application, suffering from the external force or the thermal stress generated during the phase transition, MPCMs are easily debonded from the matrix or even ruptured [16], which significantly shortens the service life of phase change composites. Therefore, increasing the mechanical strength of MPCMs and enhancing the bonding strength between MPCMs and matrix are the keys to improving the mechanical performance of composites and their lifetime.

The mechanical strength of MPCMs is mainly related to the cross-linking degree of the microcapsule shell and the ratio of shell thickness to microcapsule diameter [17]. The interface bonding strength is affected by the bonding area and the degree of molecular entanglement between MPCMs and the matrix [14]. Thus, appropriate shell material selection and the method for synthesizing microcapsule shells are crucial. In recent years, it has been favored by researchers to synthesize organic–inorganic hybrid

* Corresponding authors.
E-mail addresses: shkang@jhu.edu (S.H. Kang), piaozy@zjut.edu.cn (Z. Piao).

https://doi.org/10.1016/j.jiec.2022.03.018
1226-086X/

microcapsules by doping inorganic nanoparticles into an organic shell to combine the advantages of organic and inorganic materials [18–21]. Due to the superiorities of excellent thermal and mechanical properties, inorganic nanoparticles often play a functional role in the hybrid shell. For example, Zhang et al. [22] synthesized hybrid microcapsules with MF/hydrophobic-silicon carbide (H-SiC) as the shell by in situ polymerization. The thermal conductivity of the hybrid microcapsules with 2% H-SiC nanoparticles was increased by 55.82% compared with microcapsules without H-SiC nanoparticles.

Melamine formaldehyde (MF) resin, one of the most commonly used organic materials, has the advantages of low cost, easy preparation, and good mechanical strength [23,24]. MF resin can play a structural role in the hybrid shell. For MF shell, in situ polymerization is applied as the synthesis method. In situ polymerization forms a shell on the surface of PCMs droplets through the deposition and polymerization of MF prepolymer [25]. Titanium dioxide (TiO_2) nanoparticle, which has nontoxicity, high thermal conductivity, and outstanding mechanical property, is an excellent candidate for nanoparticle filler [26,27]. The inorganic nanoparticle fillers can be added to the emulsion system or the MF prepolymer system to synthesize organic–inorganic hybrid microcapsules [28]. For the approach of adding nanoparticles to the emulsion system, the presence of nanoparticles promotes emulsification due to the emulsifying effect of nano-scale particles [19,29]. This leads the prepared emulsion droplets to have smaller diameters. Since the forming of the microcapsule is the polymerization of MF prepolymer on the surface of core droplets, the diameter of microcapsules strongly depends on the size of the core droplets. Therefore, the prepared microcapsules have a smaller particle size at the same cumulative distribution. For the approach of adding nanoparticles to the MF prepolymer system, it has little effect on the particle size of microcapsules. However, due to the surface effect of nanoparticles, nano-TiO_2 has enormous specific surface area and surface energy, which results in a strong tendency of agglomeration of TiO_2 nanoparticles [30,31]. It is difficult for TiO_2 nanoparticles to migrate uniformly into the MF shell, which degrades the mechanical properties of microcapsules. To improve the dispersion stability of nanoparticles, it is feasible to modify nanoparticles by using silane coupling agents to lower surface energy and produce chemical bonds on the surface of nanoparticles [32–34]. In terms of matrix materials, epoxy resin is an excellent candidate due to its strong cohesiveness, good mechanical properties, and outstanding corrosion resistance. In the aerospace field, many aerospace composites are based on the blends of epoxy resin [35].

In the present work, TiO_2 nanoparticles were modified by a silane coupling agent to reduce agglomeration. Based on in situ polymerization, the modified TiO_2 nanoparticles were doped into the microcapsule shell via MF prepolymer system, forming the n-octadecane@MF/TiO_2 hybrid shell microcapsules (HS-MPCMs). The effects of nanoparticle doping on the microcapsules were analyzed from the aspects of microstructures, thermal performance, and mechanical properties.

Experimental section

Materials

Titanium dioxide (TiO_2, rutile, 99.8%) with an average size of 40 nm, as an inorganic nanofiller, was used to synthesize hybrid shells. 3-Glycidoxypropyltrimethoxysilane (KH560, ≥98.0%, Sinopharm Chemical Reagent Co., Ltd) was used to modify TiO_2 nanoparticles. n-Octadecane (99.0%) was employed as the core material. Melamine (99.0%) and formaldehyde solution (37 wt.%) were monomers for synthesizing the organic shell. Polyvinyl alcohol (PVA, 97.5–99.0 mol%) and sodium dodecyl sulfate (SDS, ≥98.5%) were used as emulsifiers. Citric acid (≥99.5%, Shanghai Macklin Biochemical Co., Ltd) and sodium hydroxide (≥96.0%, Shanghai Macklin Biochemical Co., Ltd) were applied as pH regulators. Tetraethylenepentamine (technical grade) was acted as a curing agent for the preparation of the microcapsule/epoxy composites. Without specifying, the reagents and raw materials were purchased from Shanghai Aladdin Biochemical Technology Co., Ltd.

Modification of TiO_2 nanoparticles

The purpose of modifying TiO_2 nanoparticles is to graft KH560 onto the surface of TiO_2 nanoparticles to reduce the surface energy, improve dispersion, and importantly, introduce epoxy group on the surface of TiO_2 nanoparticles. Firstly, 0.2 g of KH560 and 100 mL of deionized water were mixed in a 250 mL beaker and stirred by an overhead stirrer (DLAB OS20-Pro, China) at a speed of 200 rpm. Secondly, 2.0 g of nano-TiO_2 powder was dispersed into the above-prepared solution and the reaction was carried out at 80 °C with a stirring rate of 400 rpm for 2 h. Finally, the obtained suspension was ultrasonicated for 30 min and then the modified TiO_2 nanoparticles were collected.

Synthesis of n-octadecane@MF/TiO_2 microcapsules

In situ polymerization was applied as template for the preparation of HS-MPCMs. The schematic diagram for synthesizing HS-MPCMs was presented in Fig. 1. The preparation process was summarized as follows: (1) the synthesis of MF prepolymer solution containing modified TiO_2 nanoparticles. In a 250 mL beaker, 5.0 g of melamine was dispersed in 50 mL of deionized water, and 9.7 g of formaldehyde solution was subsequently added. The pH value of the system was adjusted to around 9.0 by the aqueous solution of sodium hydroxide (10 wt.%). The pre-experimental results showed that the prepared HS-MPCMs have good spherical shape and dispersion when the mass ratio of modified TiO_2 nanoparticles to melamine is less than 7%. Thus, 0.2 g of modified TiO_2 powder was added to the MF prepolymer system. The mixture reacted at 70 °C with a stirring rate of 250 rpm for 1 h. The obtained prepolymer suspension was stood and cooled. (2) The preparation of the Oil in Water (O/W) emulsion. The aqueous phase was prepared by 5.0 g of PVA solution (3 wt.%), 5.0 g of SDS solution (3 wt.%), and 80 mL of deionized water at 400 rpm for 5 min. Subsequently, 7.0 g of n-octadecane was added to the aqueous solution, and the mixture was emulsified by a homogenizer dispersion machine (HUXI HR-500DG, China) with a high speed of 7500 rpm at 70 °C for 20 min to obtain the O/W emulsion. The pH value of the prepared O/W emulsion was adjusted to around 4.5 by the aqueous solution of citric acid (10 wt.%). (3) The formation of microcapsule shell. The MF prepolymer suspension containing modified TiO_2 nanoparticles was added dropwise to the O/W emulsion at a rate of 1 mL/min using a separatory funnel. During the dropping process, the reaction system was stirred with a rate of 400 rpm at 65 °C, and the pH value of the reaction system was maintained in the range of 4.5–5.0. After the completion of dropping the prepolymer suspension, the temperature was raised to 70 °C, and the reaction lasted for 3 h. The prepared HS-MPCMs were then filtered, washed, and dried. The preparation of MF shell microcapsules (MS-MPCMs) follows a similar process. The only difference is the absence of modified TiO_2 nanoparticles in the prepolymer system.

Preparation of microcapsule/epoxy composites

The microcapsule/epoxy composites were prepared according to the following steps: firstly, a certain number of prepared micro-

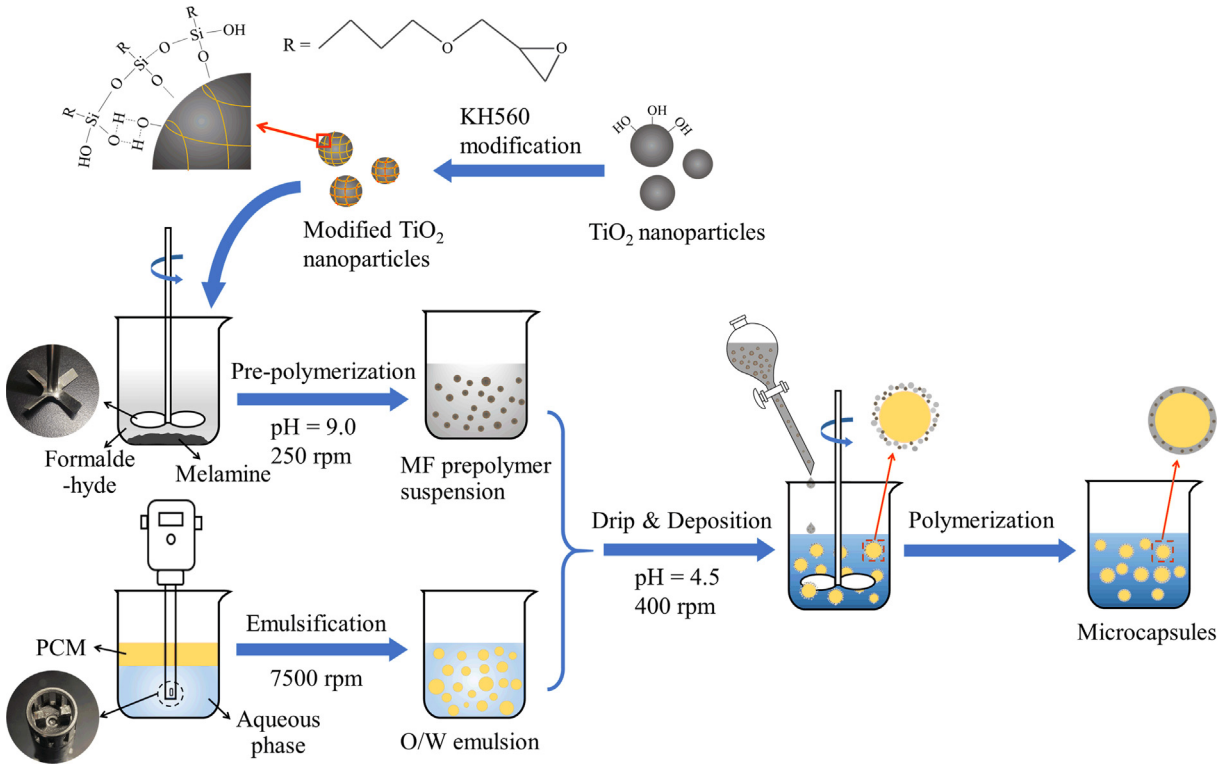

Fig. 1. The schematic diagram for synthesis of HS-MPCMs.

capsules were uniformly dispersed in the viscous epoxy resin using a vacuum deaeration mixer (SMIDA TMV-310T, China) at 1300 rpm for 5 min. Secondly, the curing agent (tetraethylenepentamine) with a mass ratio of 14 wt.% to epoxy resin was added to the microcapsule/epoxy mixture. The mixture was agitated at 1300 rpm in a vacuum for 3 min for homogeneous mixing and degassing. Finally, the mixture was poured into the dumbbell-shaped sample mold and cured at room temperature for 72 h. Four batches of microcapsule/epoxy composites with different microcapsule contents, i.e. 5%, 10%, 15%, and 20%, were prepared.

Characterization

The chemical structure of the nanoparticles and microcapsules was investigated by Fourier transform infrared spectroscopy (FTIR, Nicolet 6700 + Continuum, USA). A scanning electron microscope (SEM, Zeiss SIGMA HV-01-043, Germany) was employed to observe the morphology and microstructure of microcapsules. A laser scanning confocal microscope (Olympus OLS4500, Japan) was used to observe the optical morphology of microcapsules after micro-compression. The elemental composition and content were determined at 15 keV by an energy dispersive spectrometer (EDS, Bruker Nano Xflash Detector 5010, Germany) combined with SEM. A laser granularity analyzer (LA, HORIBA LA-950, Japan) was utilized to measure the particle size distribution of microcapsules. The thermal properties were detected by a differential scanning calorimeter (DSC, TA DSC25, USA) in the range of 0–60 °C in a nitrogen atmosphere with a heating and cooling rate of 5 °C/min. The thermal stability of the microcapsules was characterized by a thermal gravimetric analyzer (TGA, TA TGA55, USA) at a heating rate of 10 °C/min from 20 °C to 600 °C in a nitrogen atmosphere.

A nanoindentation system (Agilent Nano Indenter G200, USA) with a flat-ended indenter was employed to compress a single microcapsule and detect the rupture force [36]. The maximum compression load was set to 10 mN, and the loading time was 30 s. Based on the statistical results of microcapsule particle size, representative microcapsules with a diameter of 30 ± 1.5 μm which is close to the median diameter were picked out for the micro-compression test. For each type of microcapsules, at least five samples were tested to ensure repeatability and reliability.

The tensile strength of the microcapsule/epoxy composites was measured by a universal material testing machine (Instron E10000, USA). Four groups of the microcapsule/epoxy composites with microcapsule content of 5%, 10%, 15%, and 20% were cast into dumbbell-shaped specimens. The thickness and width within the gauge length of the specimens are 3 mm and 5 mm, respectively. The gauge length is 20 mm. For each group of the microcapsule/epoxy composites, at least four specimens were tested at a tensile strain rate of 5.5×10^{-4} s^{-1}.

Results and discussion

Chemical characterization of nanoparticles and microcapsules

The FTIR spectra of TiO_2, modified TiO_2, n-octadecane, MS-MPCMs, and HS-MPCMs were shown in Fig. 2. In the spectra of TiO_2 and modified TiO_2 nanoparticles, the absorption peaks around 530–850 cm^{-1} belong to Ti-O stretching vibration and Ti-O-Ti bridging stretching vibration [20]. The spectrum of TiO_2 displays a broad peak in the range of 3200–3600 cm^{-1}, which is attributed to the stretching vibration of the hydroxyl group on the surface of TiO_2 nanoparticles [37]. However, in the spectrum of modified TiO_2, the absorption peak corresponding to the hydroxyl group is hardly detected. In addition, the characteristic absorption peak of KH560 at 1260 cm^{-1} is presented in the spectrum of modified TiO_2 [38]. The modification mechanism is the condensation between the silanol bond of hydrolysate of KH560 and the hydroxyl group on the surface of TiO_2. It indicates that KH560 has grafted onto the surface of TiO_2 nanoparticles.

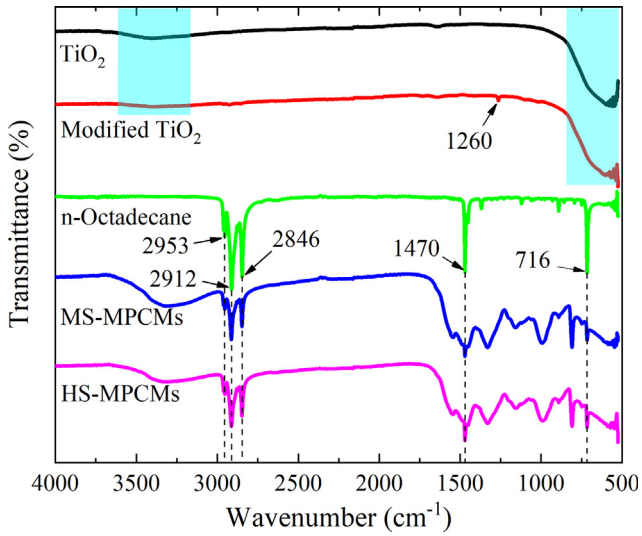

Fig. 2. The FTIR spectrums of TiO_2, the modified TiO_2, n-octadecane, MS-MPCMs, and HS-MPCMs.

For the spectrum of n-octadecane, the absorption peaks at 2953 cm^{-1}, 2912 cm^{-1}, and 2846 cm^{-1} are assigned to the aliphatic C–H stretching vibration. The peak at 1470 cm^{-1} is attributed to methylene bending vibration. The peak at 716 cm^{-1} is attributed to in-plane methylene rocking vibration [39–41]. In both spectra of MS-MPCMs and HS-MPCMs, the five characteristic peaks of n-octadecane can be easily found. Thus, it demonstrates that the n-octadecane has been successfully encapsulated.

Fig. 3 presents the EDS spectra of the modified TiO_2 and HS-MPCMs. The detection areas were marked by red circles. In the EDS spectrum of the modified TiO_2, the characteristic peak of the Si element is detected, and the Si content is 3.80 wt.%. It provides direct evidence for the successful modification of TiO_2 by KH560. The Si (0.85 wt.%) and Ti (8.92 wt.%) peaks also appear in the EDS spectrum of HS-MPCMs, indicating that the modified TiO_2 nanoparticles were successfully doped into the microcapsule shell.

Microstructures and size distribution of microcapsules

Fig. 4 shows the SEM micrographs of TiO_2 nanoparticles, modified TiO_2 nanoparticles, MS-MPCMs, HS-MPCMs, and cross-section of microcapsule shells. As marked by the red circle in Fig. 4(a), the original TiO_2 nanoparticles exhibit severe agglomeration. It can be observed from Fig. 4(b) that the agglomeration of the modified TiO_2 nanoparticles is effectively reduced after the KH560 modification. It means the KH560 grafted on the surface of TiO_2 lowers the surface energy of TiO_2 nanoparticles and hinders the aggregation between nanoparticles [30]. In Fig. 4(c) and (d), the majority of MS-MPCMs and HS-MPCMs exhibit spherical shapes with good dispersion. The enlarged views of the surface of MS-MPCMs and HS-MPCMs in Fig. 4(e) and (f) indicate that these two kinds of microcapsules have a grainy surface. It can be explained from the process of shell forming, as shown in Fig. 1. During the process of dropping MF suspension, MF prepolymer undergoes condensation to form nano-scale insoluble MF particles in the acidic system. The MF particles deposit on the surface of core droplets. As the reaction proceeds, the polymerization occurs among MF particles on the surface of core droplets to form a microcapsule shell. Compared with HS-MPCMs, the MF particles on the surface of MS-MPCMs show a higher cross-linking degree, resulting in a relatively smoother surface. The presence of modified TiO_2 nanoparticles in the surface hinders the polymerization of MF particles to form a linked surface, thus increasing the roughness of the surface for HS-MPCMs. And rough surface could be beneficial to the interface bonding between microcapsules and matrix.

The microstructures of the crushed microcapsules were also observed. As shown in Fig. 4(g) and (h), these two kinds of microcapsules have ideal core–shell structures for encapsulation of n-octadecane. After observing the dozens of broken microcapsules with diameters ranging from 20 μm to 40 μm by an SEM, the shell thicknesses of MS-MPCMs and HS-MPCMs were found to close to each other (about 1.2 μm). It means the doping of modified TiO_2 nanoparticles in the shell has little influence on the shell thickness. The particle size distributions of MS-MPCMs and HS-MPCMs were analyzed and illustrated in Fig. 5. The median diameters (D50) of MS-MPCMs and HS-MPCMs are 27.84 μm and 27.70 μm, respectively. The particle size of MS-MPCMs ranges from D3 of 0.98 μm to D97 of 64.35 μm and that of HS-MPCMs ranges from D3 of 1.00 μm to D97 of 63.26 μm. There is no obvious difference in particle size for microcapsules with and without modified TiO_2 nanoparticles. It indicates that adding modified TiO_2 nanoparticles to the MF prepolymer system can successfully yield MF/TiO_2 hybrid shell microcapsules with little effect on the geometric dimensions of microcapsules.

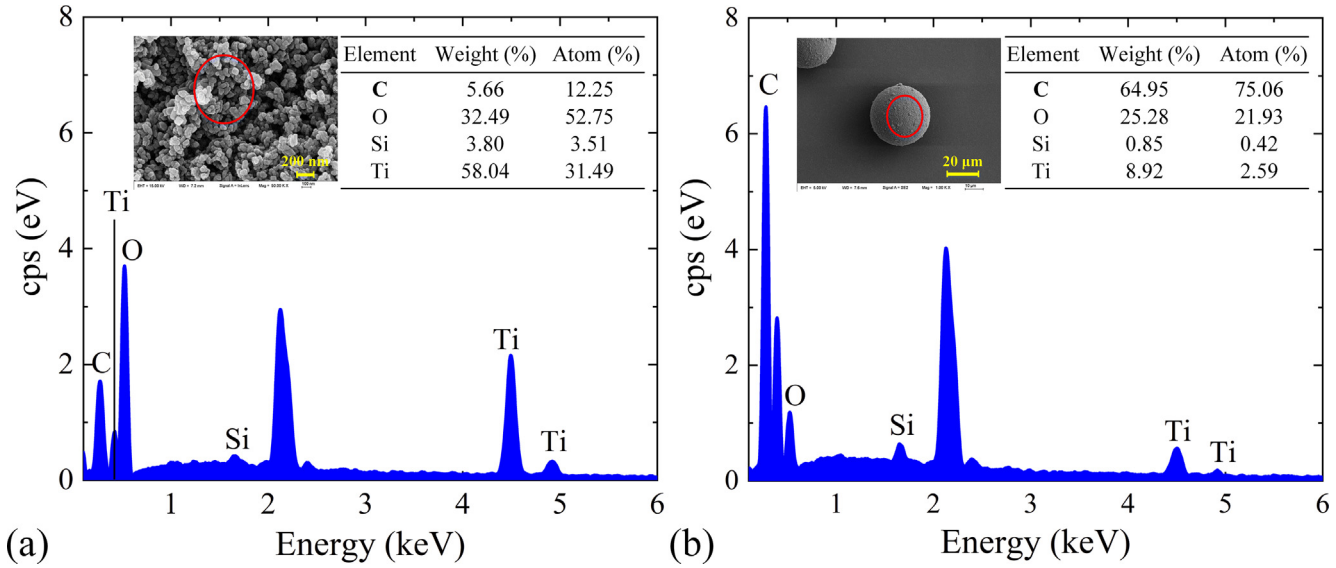

Fig. 3. EDS spectrums of (a) the modified TiO_2 and (b) HS-MPCMs.

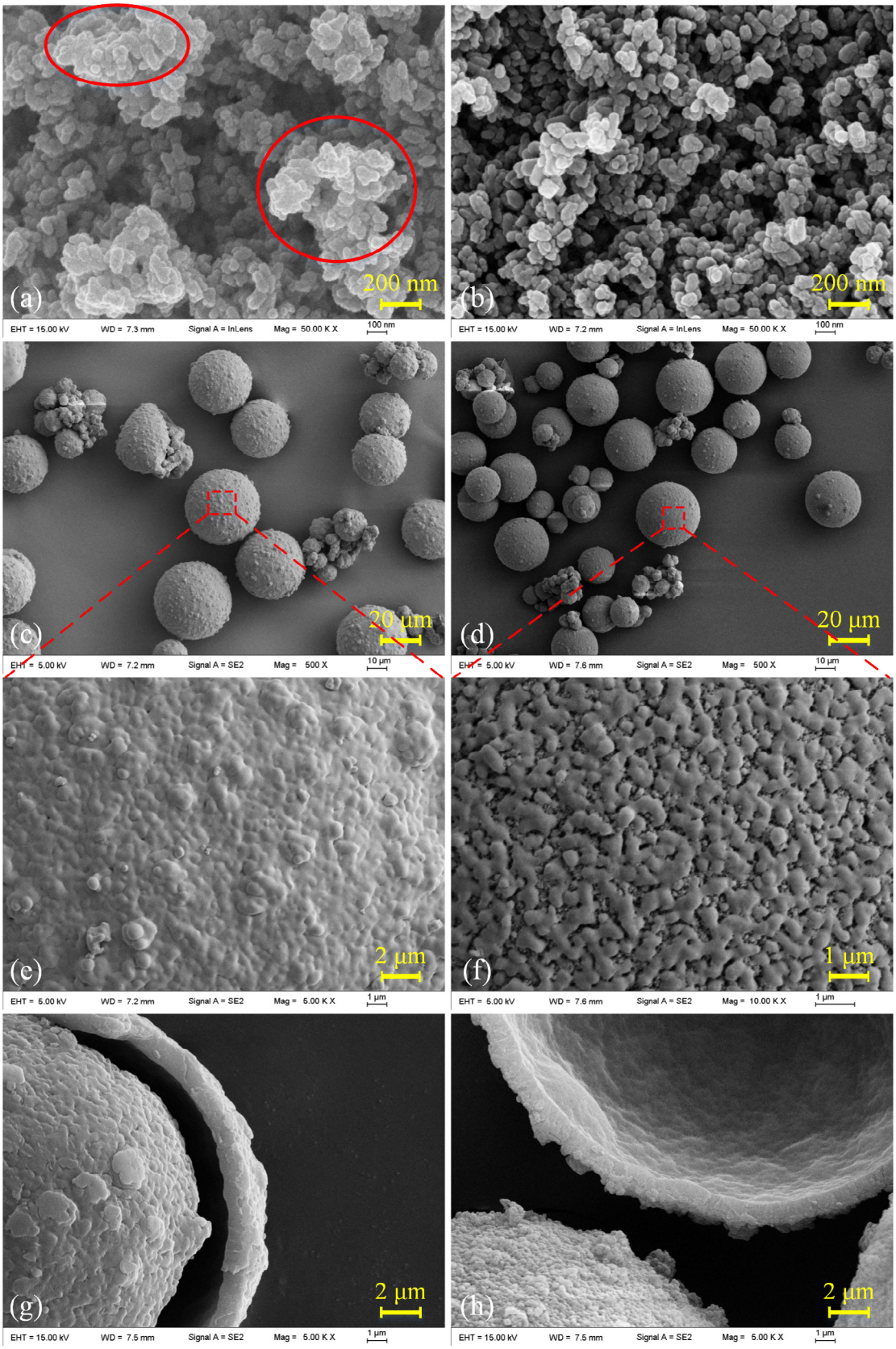

Fig. 4. SEM micrographs of (a) TiO_2 nanoparticles; (b) the modified TiO_2 nanoparticles; (c) MS-MPCMs; (d) HS-MPCMs; (e) the enlarged view of the surface of MS-MPCMs; (f) the enlarged view of the surface of HS-MPCMs; (g) the cross-section of MS-MPCMs after rupture; (h) the cross-section of HS-MPCMs after rupture.

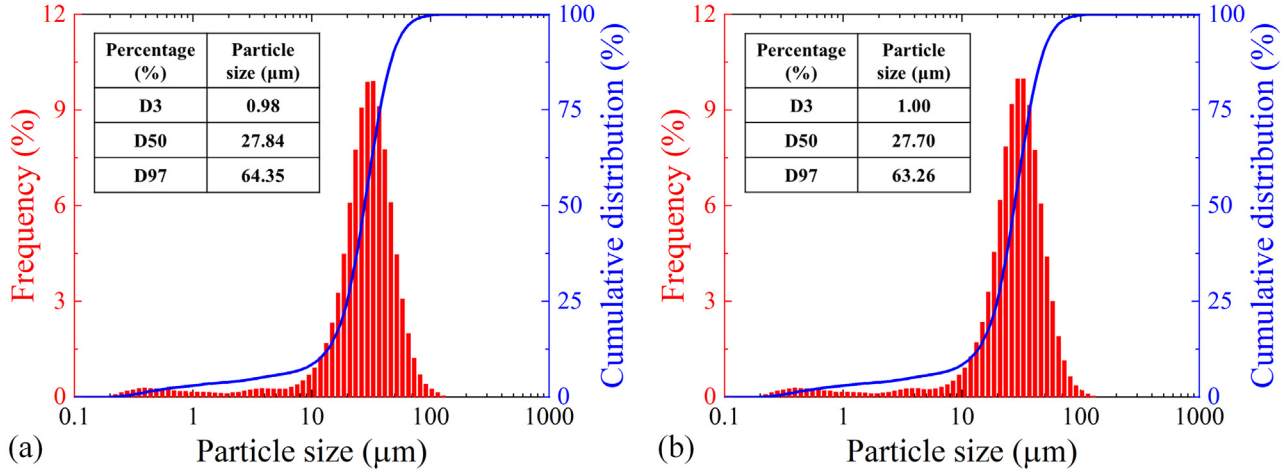

Fig. 5. Particle size distribution of (a) MS-MPCMs and (b) HS-MPCMs.

Thermal properties of microcapsules

Fig. 6 shows the DSC curves of n-octadecane, MS-MPCMs, and HS-MPCMs. And the detailed analysis results of all samples were listed in Table 1. In Fig. 6, the exothermic peaks of crystallization for MS-MPCMs and HS-MPCMs are significantly leftward in comparison with that of n-octadecane. The crystallization onset temperatures of n-octadecane, MS-MPCMs, and HS-MPCMs are 26.2 °C, 23.8 °C, and 22.8 °C, respectively. It is attributed to the fact that the phase change behavior is limited by the space inside the microcapsules [42]. Besides, both supercooling degrees (ΔT) of MS-MPCMs and HS-MPCMs are 9.4 °C and 8.4 °C. The decrease of the supercooling degree indicates that the existence of the modified TiO_2 nanoparticles might be beneficial for promoting the nucleation of liquid n-octadecane. As mentioned earlier, the microcapsule shell of HS-MPCMs is relatively rough. This core–shell interface provides the ideal sites for the nucleation of n-octadecane [37].

The melting and crystallization enthalpy of pure n-octadecane are 237.5 J/g and 238.5 J/g, respectively. The core content, C_{core}, can be calculated through the equation as follows:

$$C_{core} = \frac{\Delta H_{m,MPCMs} + \Delta H_{c,MPCMs}}{\Delta H_{m,core} + \Delta H_{c,core}} \times 100\% \quad (1)$$

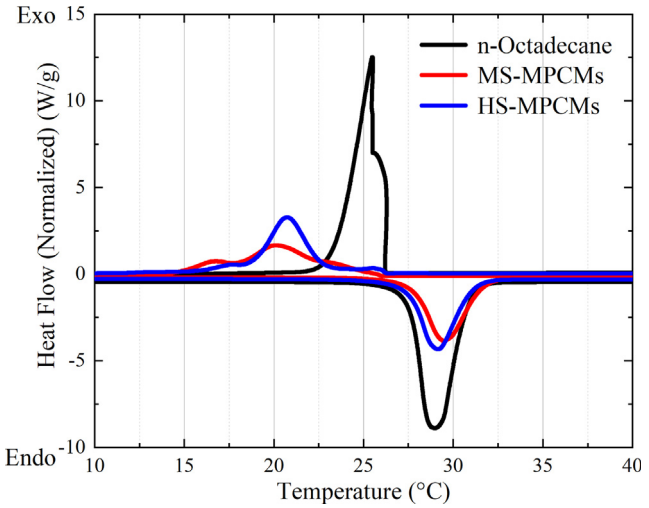

Fig. 6. DSC curves of n-octadecane, MS-MPCMs and HS-MPCMs.

where $\Delta H_{m,MPCMs}$ and $\Delta H_{c,MPCMs}$ represent the melting enthalpy and crystallization enthalpy of microcapsules, respectively. $\Delta H_{m,core}$ and $\Delta H_{c,core}$ represent the melting enthalpy and crystallization enthalpy of n-octadecane, respectively. After calculation, the core contents of MS-MPCMs and HS-MPCMs are 50.4% and 51.6%, respectively. This indicates that the doping of modified TiO_2 nanoparticles has a negligible effect on the core content of microcapsules.

The TGA curves of n-octadecane, MS-MPCMs, and HS-MPCMs were presented in Fig. 7. The TGA curve of n-octadecane presents a one-step decomposition corresponding to the volatilization of n-octadecane. The n-octadecane begins to decompose at about 100 °C and is completely decomposed at about 218 °C. The TGA curves for MS-MPCMs and HS-MPCMs exhibit a five-step decomposition: (1) The weights of MS-MPCMs and HS-MPCMs decrease slightly within the range of 50–100 °C due to the evaporation of water remaining in the samples. (2) From 150 °C to 205 °C, the curves of MS-MPCMs and HS-MPCMs show a significant drop, which corresponds to the volatilization of n-octadecane in broken or defective microcapsules. (3) When the temperature exceeds 205 °C, the MF shell begins to decompose. The mass-loss rate of HS-MPCMs is slower than that of MS-MPCMs, indicating that the MF/TiO_2 hybrid shell can provide better protection for the core materials. (4) When the temperature reaches 375 °C, the weight of MS-MPCMs drops sharply. This is because the MF shells are not strong enough to resist the pressure generated by internal gaseous n-octadecane with the decomposition of MF. The microcapsules burst and the encapsulated gaseous n-octadecane escaped rapidly. For HS-MPCMs, the sharp drop temperature is about 25 °C higher than that of MS-MPCMs. Moreover, the residual weight of HS-MPCMs is greater than that of MS-MPCMs in the temperature range of 205–400 °C. It also indicates that the HS-MPCMs have better thermal stability than the unmodified microcapsules. The reason is that the modified TiO_2 nanoparticles are uniformly distributed in the MF shell, and the presence of modified TiO_2 nanoparticles can improve the mechanical properties of microcapsules through the toughening effect. Interpretation will be detailed in Section 3.4. (5) After the sharp drop, the residual weights of MS-MPCMs and HS-MPCMs decrease at a steady rate. This process is corresponding to the decomposition of the remained MF shells. The decreasing rate is similar to that in the temperature range of 205–400 °C, indicating that the decomposition of MF shell is predominant in the range of 205–400 °C. At the end temperature (600 °C), the residual weight of HS-MPCMs is slightly higher than that of MS-MPCMs. The extra part is attributed to TiO_2 nanoparticles which are hardly decomposed below 600 °C.

Table 1
DSC analyses for n-octadecane and prepared microcapsules.

Sample	ΔH_m (J/g)	T_{om} (℃)	T_{pm} (℃)	ΔH_c (J/g)	T_{oc} (℃)	T_{pc} (℃)	ΔT (℃)	C_{core} (%)
n-Octadecane	237.5	27.6	29.0	238.5	26.2	25.5	3.5	100.0
MS-MPCMs	120.5	27.7	29.5	119.3	23.8	20.1	9.4	50.4
HS-MPCMs	123.1	27.5	29.2	122.4	22.8	20.8	8.4	51.6

Note: ΔH_m is melting enthalpy; T_{om} is melting onset temperature; T_{pm} is melting peak temperature; ΔH_c is crystallization enthalpy; T_{oc} is crystallization onset temperature; T_{pc} is crystallization peak temperature; $\Delta T = T_{pm} - T_{pc}$, represents the supercooling degree.

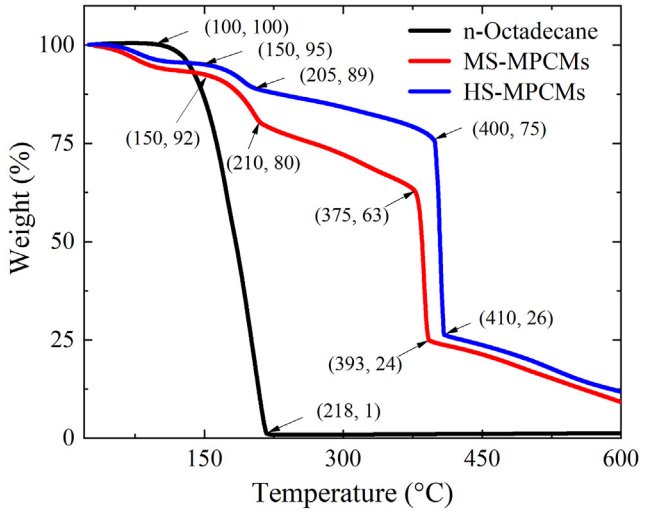

Fig. 7. TGA curves of n-octadecane, MS-MPCMs and HS-MPCMs.

Mechanical strength of microcapsules

The micro-compression curves of MS-MPCMs and HS-MPCMs were shown in Fig. 8. These curves exhibit good repeatability and have a huge pop-in plateau due to the brittle rupture of microcapsules when compression load exceeds the critical load. The compression load at the rupture point is taken as the maximum rupture load, F_m. The rupture strength is defined by the following equation [43]:

$$\sigma_m = \frac{F_m}{A} \quad (2)$$

Table 2
The rupture strength of MS-MPCMs and HS-MPCMs.

	Sample	Rupture load (mN)	Diameter (μm)	Rupture strength (MPa)
MS-MPCMs	1	4.87	29.86	6.96
	2	5.04	31.12	6.63
	3	4.63	30.01	6.55
	4	4.81	29.73	6.92
	5	4.87	29.36	7.19
Average	—	4.84 ± 0.15	—	6.85 ± 0.26
HS-MPCMs	1	6.09	29.23	9.08
	2	6.19	29.73	8.91
	3	6.08	29.32	9.01
	4	6.24	30.36	8.62
	5	6.23	29.61	9.05
Average	—	6.17 ± 0.08	—	8.93 ± 0.19

where σ_m is the rupture strength. A is the initial projection area of a microcapsule before compression test, which can be calculated by πr^2 (r indicates the radius of undeformed microcapsule).

Table 2 lists the rupture strength of MS-MPCMs and HS-MPCMs. The average rupture strength of MS-MPCMs and HS-MPCMs is 6.85 ± 0.26 MPa and 8.93 ± 0.19 MPa. It means the microcapsules with MF/TiO_2 hybrid shell have a 30.4% higher rupture strength than microcapsules with pure MF shell. Modified TiO_2 nanoparticles, as reinforcement, can form more solid shells and improve the mechanical strength of microcapsules. The reason is that when the defects or micro-cracks propagate to nanoparticles, the pinning effect of nanoparticles will increase the resistance for defect diffusion or crack propagation. Therefore, the hybrid shell microcapsules exhibit higher mechanical strength compared with unmodified microcapsules.

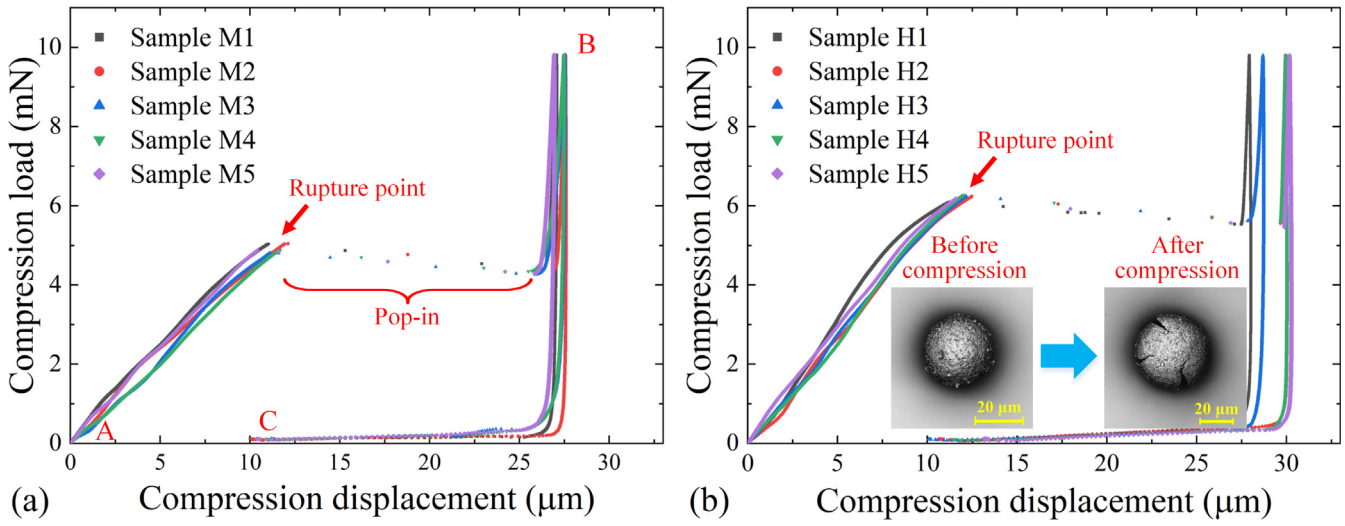

Fig. 8. The load–displacement curves of (a) MS-MPCMs and (b) HS-MPCMs with diameter of 30 ± 1.5 μm. The AB stage corresponds to the loading segment, and the BC stage corresponds to unloading segment.

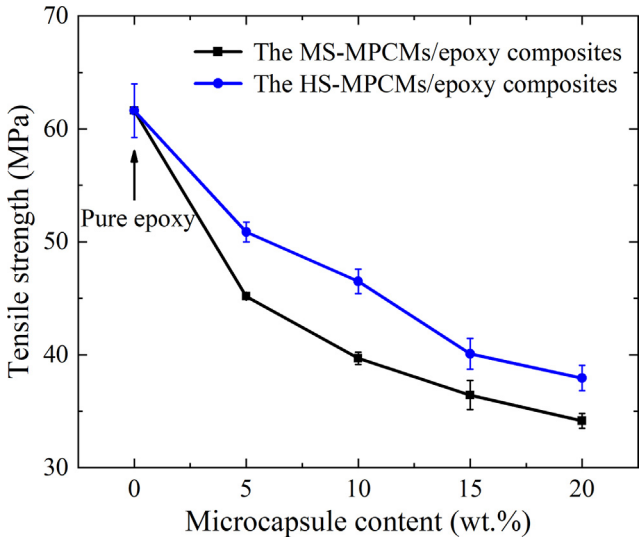

Fig. 9. Variation of tensile strength with microcapsule content for the MS-MPCMs/epoxy composites and the HS-MPCMs/epoxy composites.

Tensile strength of microcapsule/epoxy composites

Fig. 9 shows the tensile strength of the MS-MPCMs/epoxy composites and HS-MPCMs/epoxy composites with various microcapsule contents. The tensile strength of pure epoxy (without microcapsules) is 61.62 ± 2.37 MPa. For both kinds of composites, the tensile strength decreases as the microcapsule content increases. It is because microcapsules are the weak phase compared with epoxy. For the same microcapsule content, the tensile strength of HS-MPCMs/epoxy composites is higher than that of MS-MPCMs/epoxy composites. When the microcapsule content was 10 wt.%, the tensile strength of the HS-MPCMs/epoxy composites was improved by an average of 17.2%. It indicates that the doping of modified TiO_2 nanoparticles in the microcapsule shell is conducive to the enhancement of tensile strength of microcapsule/epoxy composites.

Since microcapsules are the weak phase, the mechanical strength of microcapsules and the interface bonding strength between microcapsules and epoxy are of great importance to the tensile strength of the microcapsule/epoxy composites. It can be found from Fig. 10(a) and (b) that the inner surface of the pits is smooth and no ruptured microcapsule shell remained in the pits, indicating that the MS-MPCMs were separated from the epoxy matrix without breaking. It means the bonding strength between MS-MPCMs and epoxy is weaker compared with the rupture strength of microcapsules. Thus, the debonding between microcapsules and matrix is the main failure form during the tension of MS-MPCMs/epoxy composites. In Fig. 10(c) and (d), however, rugged surface, which is the same as the inner surface of MF/TiO_2 hybrid shell as shown in Fig. 4(h), can be found in the pits. In addition, the peaks of Ti can be seen in the EDS spectrum of the inner surface of the pit, as shown in Fig. 11. It confirms that the ruptured debris of the hybrid shell remained in the epoxy matrix. It means the bonding strength between HS-MPCMs and epoxy is stronger than the rupture strength of HS-MPCMs, and microcapsule rupture is the dominant failure form during the tension of HS-MPCMs/

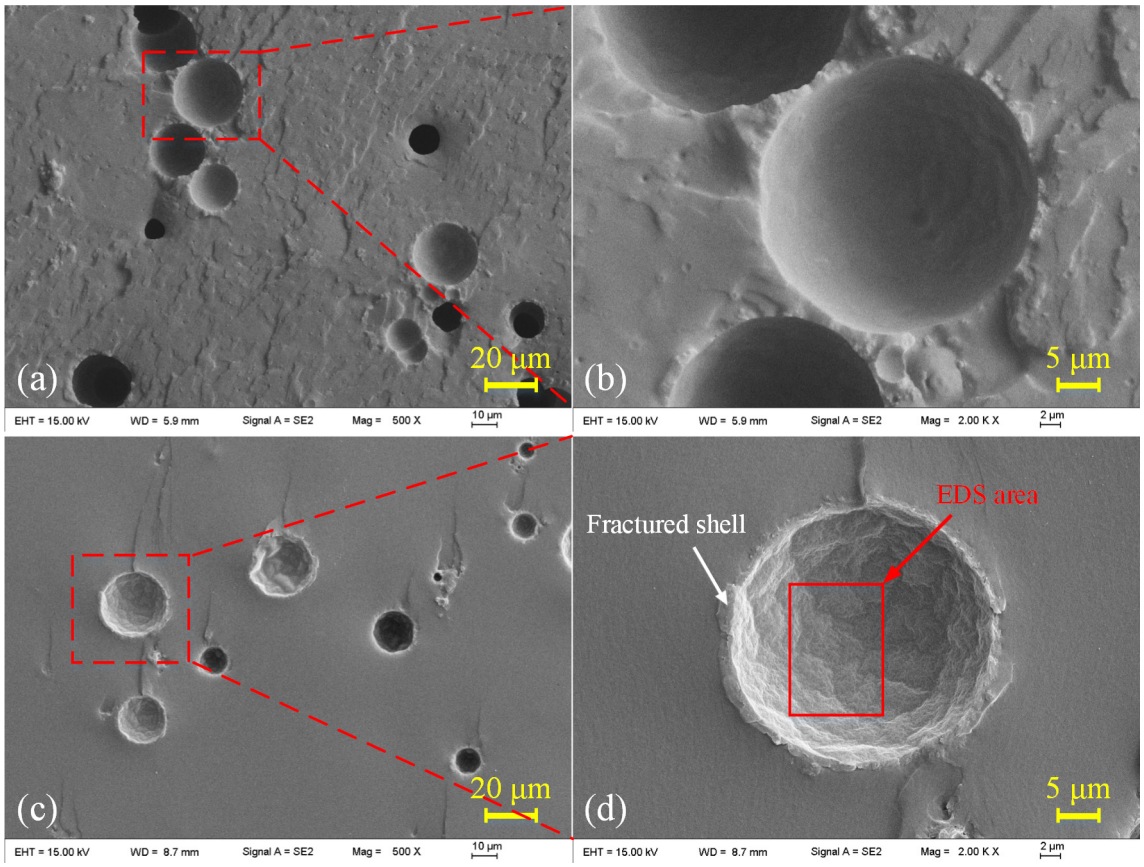

Fig. 10. SEM images for (a) the fracture surface of the MS-MPCMs/epoxy composites after tensile test; (b) the enlarged view of the pits on the fracture surface of MS-MPCMs/epoxy composites; (c) the fracture surface of the HS-MPCMs/epoxy composites after tensile test; (d) the enlarged view of the pits on the fracture surface of the HS-MPCMs/epoxy composites.

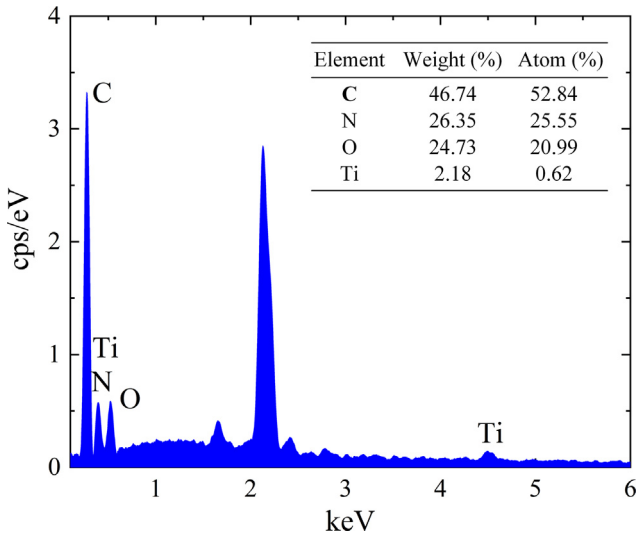

Fig. 11. EDS spectrum of the pits on the fracture surface of the HS-MPCMs/epoxy composites.

epoxy composites. As mentioned above, the mechanical strength of HS-MPCMs had been enhanced. It indirectly proves that the interface bonding strength between HS-MPCMs and epoxy was enhanced. The strengthening of the HS-MPCMs/epoxy interface is because the epoxy group grafted on the surface of modified TiO_2 nanoparticles and the epoxy group of the epoxy matrix react with the amino group of the curing agent to form covalent bonds [44]. Ultimately, the enhancement in both the mechanical strength of microcapsules and the interface bonding strength between microcapsules and epoxy improves the tensile strength of the composites.

Conclusion

Applying in situ polymerization, n-octadecane@MF/TiO_2 hybrid shell microcapsules with better mechanical properties were successfully synthesized by doping KH560 modified TiO_2 nanoparticles in the MF shell. The rupture strength of HS-MPCMs is 30.4% higher than that of pure MF shell microcapsules. The doping of modified TiO_2 nanoparticles to the MF shell also enhances the interface bonding strength between microcapsules and epoxy matrix by improving chemical bonding. The curing agent, as a molecular bridge, reacts with the epoxy group grafted on the surface of modified TiO_2 and the epoxy group of the epoxy matrix to form covalent bonds to enhance chemical bonding. Since both the rupture strength of HS-MPCMs and the interface bonding strength between HS-MPCMs and epoxy matrix were enhanced, the HS-MPCMs/epoxy composites possess higher tensile strength than the unmodified microcapsule/epoxy composites for various microcapsule contents. Furthermore, the HS-MPCMs also perform better thermal properties. The doping of the modified TiO_2 nanoparticles reduces the supercooling degree and improves the thermal stability of microcapsules. In the temperature range of 205–400 °C, the residual weight of HS-MPCMs is higher than that of MS-MPCMs. The MF/TiO_2 hybrid shell, which has higher mechanical strength, provides better protection for the core materials. It indicates that increasing the mechanical strength of the microcapsule is beneficial to the improvement of thermal stability. In summary, the addition of appropriate nanoparticles in the microcapsule shell is a simple and feasible strategy to improve both the mechanical and thermal properties of MPCMs. The hybrid shells are also conducive to the enhancement of the macro mechanical strength of MPCMs/epoxy composites. The reinforced MPCMs/epoxy composites are expected to be used as anti-icing coatings in the aerospace field.

Declaration of Competing Interest

The authors declare that they have no known competing financial interests or personal relationships that could have appeared to influence the work reported in this paper.

Acknowledgements

The authors would like to gratefully acknowledge the support from the National Natural Science Foundation of China (Grant Nos. 11772302, 12172332, 11727803 and 11972037), the Fundamental Research Funds for the Provincial Universities of Zhejiang (RF-A2020013), and the Johns Hopkins University start-up fund for Sung Hoon Kang (United States).

References

[1] A. Sharma, V.V. Tyagi, C.R. Chen, D. Buddhi, Renew. Sustain. Energy Rev. 13 (2009) 318–345.
[2] G. Peng, G. Dou, Y. Hu, Y. Sun, Z. Chen, Adv. Polym. Tech. 2020 (2020) 1–20.
[3] M. Pretzl, M. Neubauer, M. Tekaat, C. Kunert, C. Kuttner, G. Leon, D. Berthier, P. Erni, L. Ouali, A. Fery, ACS Appl. Mater. Interfaces 4 (2012) 2940–2948.
[4] Z. Sun, K. Sun, H. Zhang, H. Liu, D. Wu, X. Wang, Sol. Energy Mater. Sol. Cells 225 (2021).
[5] R. Al-Shannaq, J. Kurdi, S. Al-Muhtaseb, M. Farid, Sol. Energy 129 (2016) 54–64.
[6] G. Urgessa, K.-K. Yun, J. Yeon, J.H. Yeon, Cem. Concr. Compos. 104 (2019).
[7] J. Giro-Paloma, R. Al-Shannaq, A.I. Fernandez, M.M. Farid, Materials (Basel) 9 (2015).
[8] K.O. Lee, M.A. Medina, X. Sun, X. Jin, Sol. Energy 163 (2018) 113–121.
[9] W. Guo, Y. Jia, K. Tian, Z. Xu, J. Jiao, R. Li, Y. Wu, L. Cao, H. Wang, ACS Appl. Mater. Interfaces 8 (2016) 21046–21054.
[10] R.S. Yu, H. Yan, Z.C. Xu, Z.H. Liu, Z.D. Gu, Adv. Mater. Res. 239–242 (2011) 441–444.
[11] Y. Zhu, K. Cao, M. Chen, L. Wu, ACS Appl. Mater. Interfaces 11 (2019) 33314–33322.
[12] A. Nejman, M. Cieślak, B. Gajdzicki, B. Goetzendorf-Grabowska, A. Karaszewska, Thermochimica Acta 589 (2014) 158–163.
[13] F.A.P. Scacchetti, E. Pinto, G.M.B. Soares, J. Appl. Polym. Sci. 135 (2018).
[14] J.-F. Su, X.-Y. Wang, H. Dong, Compos. Interfaces 18 (2012) 645–659.
[15] Y. Sun, G. Peng, Y. Hu, G. Dou, P. Chen, T. Zhang, Int. J. Solids Struct. 230–231 (2021).
[16] J.-F. Su, X.-Y. Wang, S.-B. Wang, Y.-H. Zhao, K.-Y. Zhu, X.-Y. Yuan, Polym. Compos. 32 (2011) 810–820.
[17] F. Uebel, H. Therien-Aubin, K. Landfester, Nanoscale 13 (2021) 15415–15421.
[18] C. Li, H. Yu, Y. Song, H. Liang, X. Yan, Energy 167 (2019) 1031–1039.
[19] D. Yin, H. Liu, L. Ma, Q. Zhang, Polym. Adv. Technol. 26 (2015) 613–619.
[20] X. Sheng, D. Xie, C. Wang, X. Zhang, L. Zhong, Colloid Polym. Sci. 294 (2015) 463–469.
[21] S. Parvate, J. Singh, J. Reddy Vennapusa, P. Dixit, S. Chattopadhyay, J. Ind. Eng. Chem. 102 (2021) 69–85.
[22] B. Zhang, S. Li, X. Fei, H. Zhao, X. Lou, Colloids Surf. A: Physicochem. Eng. Aspects 603 (2020).
[23] Z. Chen, J. Wang, F. Yu, Z. Zhang, X. Gao, J. Mater. Chem. A 3 (2015) 11624–11630.
[24] R. Huang, W. Li, J. Wang, X. Zhang, New J. Chem. 41 (2017) 9424–9437.
[25] D. Yin, L. Ma, W. Geng, B. Zhang, Q. Zhang, Int. J. Energy Res. 39 (2015) 661–667.
[26] E. Džunuzović, M. Marinović-Cincović, J. Vuković, K. Jeremić, J.M. Nedeljković, Polym. Compos. 30 (2009) 737–742.
[27] Y. Zhang, Y. Wu, M. Chen, L. Wu, Colloids Surf. A: Physicochem. Eng. Aspects 353 (2010) 216–225.
[28] Y. Sun, R. Wang, X. Liu, M. Li, H. Yang, B. Li, J. Appl. Polym. Sci. 134 (2017).
[29] X. Wang, C. Li, T. Zhao, Sol. Energy Mater. Sol. Cells 183 (2018) 82–91.
[30] C. Wang, H. Mao, C. Wang, S. Fu, Ind. Eng. Chem. Res. 50 (2011) (1934) 11930–11931.
[31] S. Kango, S. Kalia, A. Celli, J. Njuguna, Y. Habibi, R. Kumar, Prog. Polym. Sci. 38 (2013) 1232–1261.
[32] Y. Rong, H.-Z. Chen, G. Wu, M. Wang, Mater. Chem. Phys. 91 (2005) 370–374.
[33] X. Li, D. Wang, Q. Luo, J. An, Y. Wang, G. Cheng, J. Chem. Technol. Biotechnol. 83 (2008) 1558–1564.
[34] B. Jiang, X. Zu, F. Tang, Z. Wu, J. Lu, Q. Wei, X. Zhang, J. Appl. Polym. Sci. 100 (2006) 3510–3518.
[35] J.P. Foreman, D. Porter, S. Behzadi, P.T. Curtis, F.R. Jones, Compos. Part A: Appl. Sci. Manuf. 41 (2010) 1072–1076.
[36] G. Peng, Y. Sun, G. Dou, Y. Hu, W. Jiang, T. Zhang, Langmuir 36 (2020) 5176–5185.

[37] J. Zhao, Y. Yang, Y. Li, L. Zhao, H. Wang, G. Song, G. Tang, Sol. Energy Mater. Sol. Cells 168 (2017) 62–68.
[38] X.L. Cai, D.T. Fu, A.L. Qu, Plastics Rubber Compos. 43 (2014) 161–165.
[39] X. Qiu, W. Li, G. Song, X. Chu, G. Tang, Sol. Energy Mater. Sol. Cells 98 (2012) 283–293.
[40] X.L. Shan, J.P. Wang, X.X. Zhang, X.C. Wang, Thermochim. Acta 494 (2009) 104–109.
[41] Z. Liu, Z. Chen, F. Yu, Sol. Energy Mater. Sol. Cells 192 (2019) 72–80.
[42] H. Zhang, X. Wang, Colloids Surf. A: Physicochem. Eng. Aspects 332 (2009) 129–138.
[43] Y. Zhang, Y. Zhao, F. Wu, X. Zhang, Z. Zhang, Y. Xiang, J. Yang, Int. J. Mech. Sci. 205 (2021).
[44] R. Wang, H. Li, W. Liu, X. He, J. Macromol. Sci., Part A 47 (2010) 991–995.